11th International Symposium on Turbulence and Shear Flow Phenomena (TSFP11)
Southampton, UK, July 30 to August 2, 2019

SPATIAL CHARACTERISTICS OF SCALAR DISSIPATION RATE IN STEADY AND UNSTEADY TURBULENT ROUND JETS

Vlad Aparece-Scutariu
School of Engineering
University of Edinburgh
Edinburgh, EH9 3FD, United Kingdom
V.Aparece-Scutariu@ed.ac.uk

Edward S Richardson
Faculty of Engineering and Physical Sciences
University of Southampton
Southampton, SO17 1BJ, United Kingdom
E.S.Richardson@soton.ac.uk

Dong-hyuk Shin
School of Engineering
University of Edinburgh, Edinburgh, EH9 3FD, United Kingdom
Korea Advanced Institute of Science and Technology, 34141, South Korea
d.shin@ed.ac.uk

ABSTRACT

This paper investigates the characteristics of mixture fraction scalar dissipation rate (SDR) in statistically-steady and starting turbulent round jets using Direct Numerical Simulations (DNS). The SDR quantifies the rate of mixing between the jet and the ambient fluids and is a key parameter for modelling turbulent combustion processes such as ignition and extinction. For the steady-state jet, radial profiles of ensemble-averaged SDRs exhibit self-similar behaviour. The self-similar radial profile of the ensemble-averaged SDR exhibits a core of fluid with uniformly-high SDR around the centerline, beyond which the averaged SDR decays in the radial direction. Previous modelling for ensemble-averaged SDR profile is found to give large errors around the jet centreline due to neglect of mixing in the axial direction. The ensemble-averaged SDR in the head of the starting jet exceeds the steady-state value by a factor of three. Behind the leading vortex, the SDR profile narrows and drops below steady state value, only relaxing towards the steady state value once the head of the jet has passed many jet widths further downstream.

INTRODUCTION

Characterisation of scalar mixing in turbulent jets remains a complex problem, yet fundamentally important for understanding the basic processes occurring in many applications such as combustion, pollutant emissions from industrial smokestacks or volcanic eruptions. In combustion applications, two streams of fluids, fuel and oxidizer, are introduced in a combustion chamber and combustion performance is sensitive to the rate of mixing and to the spatial distribution of the mixture.

Mixing processes in combustion are characterised by the mixture fraction and its scalar dissipation rates (SDR). Mixture fraction, denoted as ξ, is a conserved scalar defined as the fraction of the fluid mass originating from the fuel stream. Scalar dissipation rate, denoted by χ, represents the rate of mixing, related by the gradient of the mixture fraction. For a mixture with equal diffusivities $\mathscr{D}$ for all chemical species, SDR is defined as

$$\chi = 2\mathscr{D}(\nabla\xi)^2 \tag{1}$$

In non-premixed combustion systems, where the rate of chemical reaction is limited by the rate of mixing of fuel and oxidiser, the ensemble-average SDR is directly related to the mean reaction rate (Bilger, 1976). SDR also characterises how the turbulent straining of the fluid affects chemical processes within the flame (Williams,1975; Peters,1984) and thereby has a critical influence on extinction and ignition phenomena (Mastorakos *et al.*, 1997). Turbulent combustion models utilizing SDR may also make use of additional submodels for conditionally-averaged SDR and a presumed probability density function for SDR.

Mixing in starting and pulsed jets is of particular importance for the fuel-injection process in diesel engines where the unsteady nature of the fuel jet enhances entrainment of surrounding air (Hill & Greene, 1977; Bremhorst & Hollis, 1990). The enhanced entrainment is desirable as it leads to a reduction in soot formation. However excessive mixing may prevent complete combustion. Thus, in order to optimise the fuel injection process, it is therefore important to understand the mixing dynamics as the fuel injection starts.

Turbulence acts to fold and stretch the diffusive interface between different fluid streams, producing thin structures with relatively high scalar dissipation rate. Repeated folding and stretching of the scalar interface would act to increase scalar gradients exponentially, until the scalar length scale reduces to a viscous limit such as the Batchelor or Kolmogorov scale, resulting in a log-normal distribution of SDR (Oboukhov, 1962; Kolmogorov, 1962). The probability density function (PDF) of SDR for passive scalars has been found to be approximately log-normal in round turbulent jets, with deviations attributed to anisotropy (Feikema *et al.*, 1996). Additional deviations from the log-normal distribution scalar dissipation rate arise in the case of chemically-reacting scalars for which reaction generates

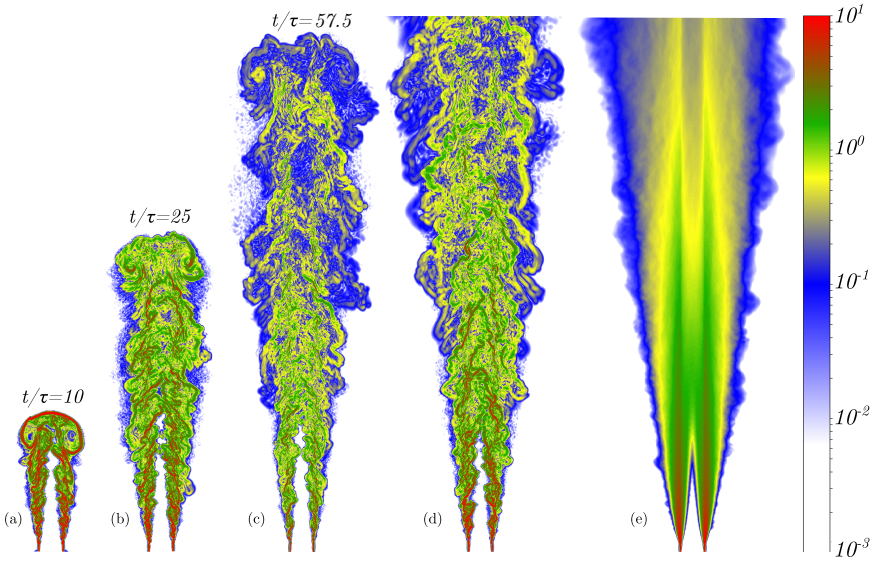

Figure 1: Non-dimensionalised scalar dissipation rate: $(a)-(c)$ starting jet time instances, (d) steady state instantaneous snapshot, (e) steady state time-averaged.

steep gradients at small scales (Richardson *et al.*, 2010).

Measuring SDR experimentally in turbulent flows is challenging because it requires measurement of three components of the scalar gradient within structures that are similar in size to the Kolmogorov or Batchelor scales. Furthermore, such measurements are prone to experimental noise (Soulopoulos *et al.*, 2014). Notwithstanding these difficulties, numerous diagnostic developments have contributed to the measurements of passive and reactive scalar gradients in one (Antonia & Mi,1993; Barlow *et al.*, 2001) or two dimensions (Kaiser & Frank, 2007). However, for a complete description of scalar mixing, measurements in three dimensions are necessary, yet these remain a difficult task to carry out experimentally.

Peters & Williams (1983) proposed a model for the ensemble-averaged SDR assuming that it can be related to the gradient of the ensemble-averaged mixture fraction. The key features of the model are: (i) employing a turbulent diffusivity (ν_t/Sc_t) and (ii) assuming the derivatives in the streamwise and azimuthal directions are negligible, leading to

$$\overline{\chi} = \frac{2\nu_t}{Sc_t}\left(\frac{\partial\overline{\xi}}{\partial r}\right)^2, \qquad (2)$$

where Sc_t is the turbulent Schmidt number and ν_t is the turbulent kinematic viscosity.

In turbulent combustion such as diffusion flames, the local strain rate is an important feature to consider, since turbulence acts to stretch and contort the thin reaction sheets. If the value of local strain rate exceeds a certain threshold (Linan, 1974), the reaction can abruptly stop, hence local flame extinction occurs. Peters & Williams (1983) have shown that mixture fraction (ξ) and scalar dissipation (χ) can be related to the local strain rate. Thus, by knowing the joint PDF shape of the two variables, is possible to account for strain rate effects in existing mixing models (Roomina & Bilger, 2001).

DNS data are valuable complements since the scalar field is available instantaneously in three-dimensions at a wide range of locations. Furthermore, data are required in order to investigate the evolution of SDR in response to a starting jet.

SIMULATION SETUP/FORMULATION

The simulations are conducted using a compressible DNS code, HiPSTAR (Sandberg & Tester, 2016). The flow domain uses a structured grid stretched in the downstream direction with a cylindrical configuration. A 5^{th} order finite difference scheme is used for the stream-wise and radial directions, and a spectral decomposition is used in the azimuthal direction. The fluid is treated as a perfect gas, having the same temperature and density as the ambient fluid. The Reynolds number is 7 300 and the initial Mach number of the jet fluid is 0.304. Figure 1 shows a snapshot of SDR for the steady-state jet and three instances of the starting jet.

The steady-state jet is established after 540 characteristic jet times (τ) where $\tau = D/U_0$ with D as the jet inlet diameter and U_0 the inlet jet velocity. In addition to the steady-state jet, three realisations of a starting jet were simulated. For the latter, a step change in the inlet velocity occurs at time $t/\tau = 0$ from 0 to U_0. The jet is allowed to evolve for 66τ when the leading vortices reach at around $26D$ downstream. Along with the fluid flow equations, the transport equation for mixture fraction is solved and used to evaluate SDR. A more detailed description about the code and setup can be found in Shin *et al.* (2017a).

SCALAR DISSIPATION RATE CHARACTERISATION

As shown in Figure 1, SDR decreases with downstream distance. Near the inlet region, strong gradients are present, indicating intense mixing between the jet and ambient fluids. Further downstream, mixing becomes less intense, and SDR values are much decreased - note that SDR is coloured in log-scale. Moreover, the inlet region contains temporally and spatially-coherent mixing layers aligned at angles of 45° to 75° across where intense scalar mixing occurs. The angles are consistent with the observation by Feikema *et al.* (1996) who proposed that the structures appear due to rotation of vortices at the interface between the jet and ambient

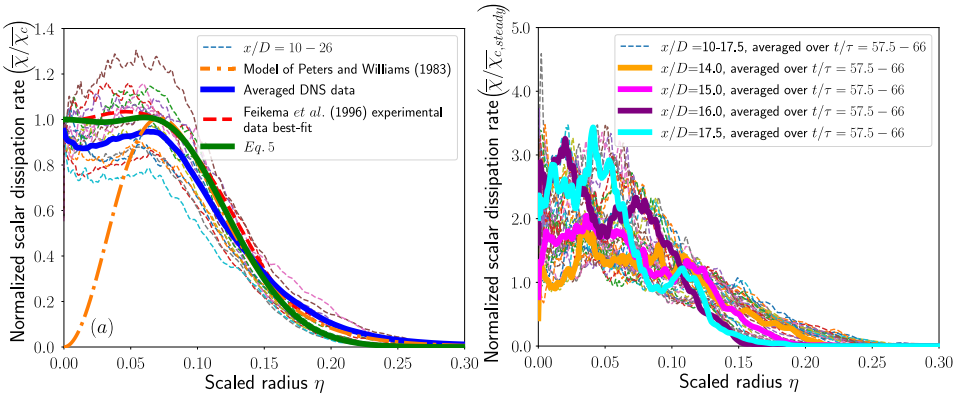

Figure 2: Radial profiles of the mean scalar dissipation normalised by centreline values for *(a)* steady-state jet and *(b)* starting jet

fluids. The rotation engulfs ambient fluid from a location that is immediately upstream of each vortex and then draws the fluid downstream. As such, strong mixing occurs at the boundary of these regions, highlighted by dark red colour in Figure 1.

Mean Scalar Dissipation Rate Radial profiles of SDRs for steady-state and starting jets are shown in Figure 2a and b. In the figures, the ensemble-averaged SDRs are scaled by their respective centreline values, denoted by $\overline{\chi_c}$. The radius is scaled by the downstream distance x, where $x = X - X_0$, X being the distance from the inlet and X_0 being the virtual origin with the value of $2.39D$ for this simulation. Note that η is the scaled radius, defined as r/x.

Figure 2a shows SDR profiles for the steady-state jet. The thin dashed lines are the profiles at different x-locations, and their average is drawn in the thick blue line. Although there are a scatter among the dashed lines, the scatter is narrow indicating that the self-similarity exists. Two main possible reasons for the scatter are: (*i*) noise in the centreline values which are used to normalise the radial profiles and (*ii*) the gradual development of self-similarity along the axial direction. Therefore, SDR profiles start to become self-similar at around x/D =10. Experimental investigations of Feikema *et al.* (1996) on a gaseous propane jet, suitable for comparison with present simulation data, indicate the same general behaviour with a decrease in dissipation in the vicinity of the centreline, followed by an increase and a peak in the shear layer region and a gradual decrease closer to the interface with ambient fluid.

Figure 2b shows the short time-averaged SDR of the starting jet. The band of time average is chosen close toward the end of the simulation, in order to make sure SDR profiles upstream of the leading vortices region tend towards a quasi-steady-state. The averaged SDR is then normalised by their respective centreline values from the steady-state jet. As estimated in Figure 1c, the leading vortices are at around x/D =16.5-17.5 at 57.5τ. Increased SDR values for the leading vortices region of the jet (at x/D=16 or 17.5) are followed by a slow decay towards steady-state jet SDR profiles (at x/D=14 or 15). The overall shape of profiles show a steeper decay with increasing radius compared to the steady-state jet. This is confirmed by observing the strong gradients in the starting jet at the leading vortices (Figure 1a-c).

For the self-similar region of the steady-state jet, an improved model for the ensemble-averaged SDR is developed. This extends from the analysis of Peters & Williams (1983) who investigates species production in turbulent diffusion flames, for very narrow temperature bands, which can be applied to non-reacting jets as well. By incorporating Eq.1 for a turbulent round jet in cylindrical coordinates (i.e. x - axial direction, r - radial, θ - azimuthal), an revised ensemble-averaged SDR model starts from:

$$\overline{\chi} = \frac{2\nu_t}{Sc_t}\left[\left(\frac{\partial\overline{\xi}}{\partial x}\right)^2 + 2\left(\frac{\partial\overline{\xi}}{\partial r}\right)^2\right], \tag{3}$$

where the axial gradient is included and the azimuthal gradient is assumed to have a magnitude similar to the radial gradient, which is also employed by Sreenivasan *et al.* (1977) and Antonia *et al.* (1983). Although the assumption would be exact in isotropic turbulence, it introduces relatively small errors when calculating time averages for turbulent steady-state jets (Feikema *et al.*, 1996).

The ensemble-averaged mixture fraction ($\overline{\xi}$) in the self-similar region can be approximated as follows:

$$\overline{\xi} = \overline{\xi}_c exp\left(-\gamma_t Sc_t \frac{\eta^2}{2}\right) \quad with \quad \overline{\xi}_c = \frac{c_1}{x/D}, \tag{4}$$

where γ_t is a fitting parameter for the self-similar profile and c_1 as a centreline decay rate which is 6.2 for the present simulation.

Plugging Eq. 3 into Eq. 4 leads to:

$$\overline{\chi} = \frac{2\nu_t}{Sc_t}\frac{\overline{\xi}_c^4}{c_1^2 D^2} f(\eta) \quad where$$
$$f(\eta) = exp\left(-\gamma_t Sc_t \eta^2\right)\left[1 - \gamma_t Sc_t \eta^2\left(2 - \gamma_t Sc_t(2+\eta^2)\right)\right]. \tag{5}$$

From the existing DNS data, γ_t is 180 and the non-dimensionalised fluid kinematic viscosity and turbulent Schmidt number are given as $\nu_t = 4.11 \times 10^{-4}$ and $Sc_t = 0.72$. As shown in Figure 2a, Eq. 5 agrees better with the mean SDR radial profile for the steady-state jet, especially in the vicinity of the centreline, while the model by Peters & Williams (1983) approaches to zero.

Statistics of Mixture Fraction and Scalar Dissipation Rate Profiles of the simple PDFs for

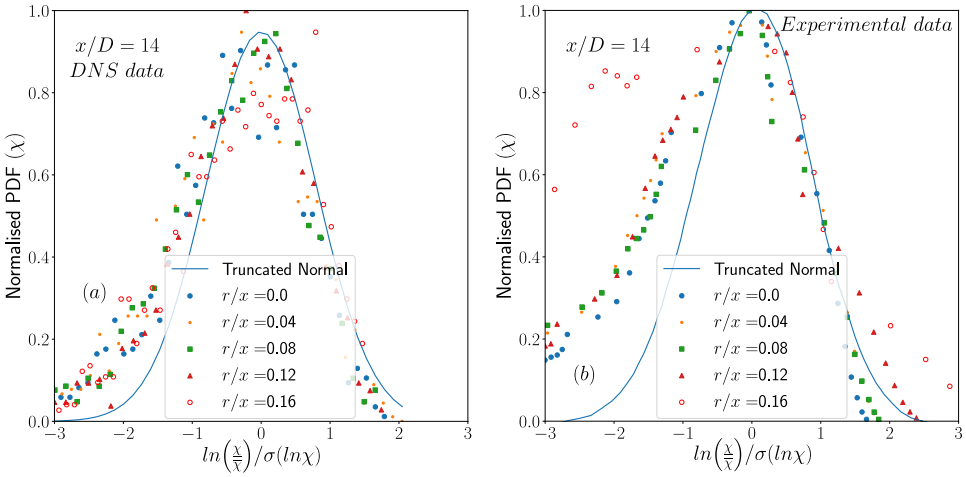

Figure 3: Steady-state jet − normalized PDFs for the SDR (χ) at fixed axial location: (a) $x/D = 10$ from DNS data, equivalent of $x/D = 14$ in Feikema *et al.* (1996), (b) $x/D = 14$ from Feikema *et al.* (1996)

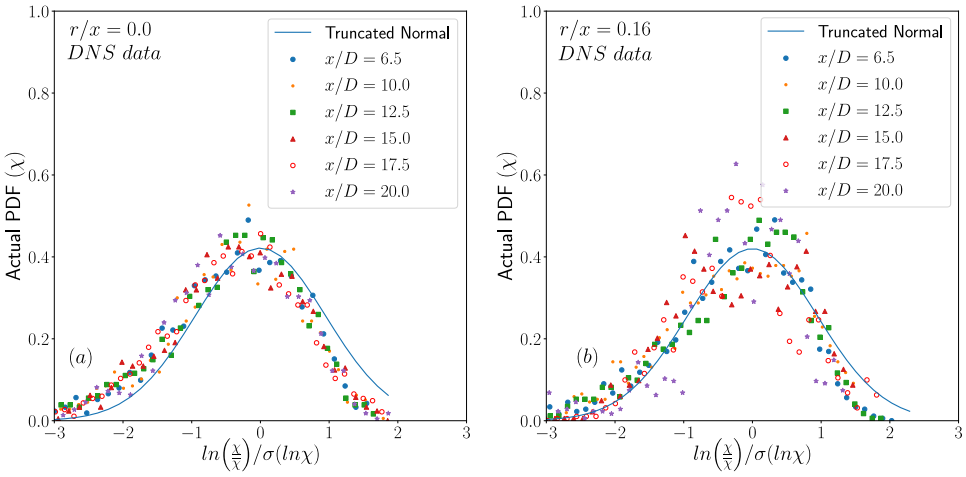

Figure 4: Steady-state jet − actual PDFs for the SDR (χ) at fixed r/x values: (c) $r/x = 0$ and (d) $r/x = 0.16$.

steady-state jet SDR are shown in Figures 3 and 4. Firstly, the sample space is normalised by the mean (μ) and the standard deviation (σ) of the logarithm of SDR. In Figure 3a and b, the PDF are normalised by the maximum probability value (P_{max} =0.49 for DNS) for consistent comparison - the experimental data of Feikema *et al.* (1996) only reported the normalized PDFs. In addition, the best-fitting truncated-normal distributions (Burkardt, 2014) are added in each figure. Overall, PDF values show a leftwards deviation from the expected log-normal distribution for both DNS and experimental data (Figure 3a-b), due to the anisotropy of dissipation layers. On top of that, the large probability associated with low scalar dissipation values highlight the increased number of homogeneous regions far from the jet inlet, which are either fully mixed or unmixed.

Figure 4 highlights the self-similarity of SDR along the axial direction for different radial locations. The same deviation from the log-normal behaviour is visible. For the outer jet region, the intermittent behaviour of the jet leads to large probability values for a wider range of SDR values as compared to regions closer to the jet centreline. This is highlighted by comparing the PDFs in Figures 4a-b, the latter displaying a more flattened peak.

Simple PDFs for the starting jet are presented using both DNS data (Figure 5a) and existing measurements (Figure 5b) of Soulopoulos *et al.* (2014). Each PDF is sampled at a certain flow location and specific time. As for the steady-state case, simple PDFs of SDR values for the starting jet show a deviation from the expected log-normal behaviour. While in the case of DNS data this deviation is less apparent, for the experimental jet, the difference can be clearly observed, because of the wider range of sampled SDR values. The computational cost of DNS simulations prohibits an increased number of jet realisations, affecting the range of collected SDR data. For the present simulation only 3 realisations have been produced, whereas experiments of Soulopoulos *et al.* (2014) contain 500 jet realisations. In terms of sampling locations, the PDF of simulation SDR values is close to the intermittent boundary between the jet and ambient fluid. This induces higher scatter in SDR values, with a plateau at large probability values, as compared to experimental results, which are sampled at a location closer to the jet centreline, hence a visible peak of the PDF.

Figure 6 shows the joint PDF of mixture fraction and SDR at x/D =15 for the steady-state jet. It can be seen that for the first three radial locations, the PDFs display symmetry with respect to mixture fraction (ξ), while at the last radial location, the symmetry is broken. Contours move down as the radial location goes towards the outer jet regions as $\overline{\xi}$ decreases. Qualitatively, joint PDFs of DNS data

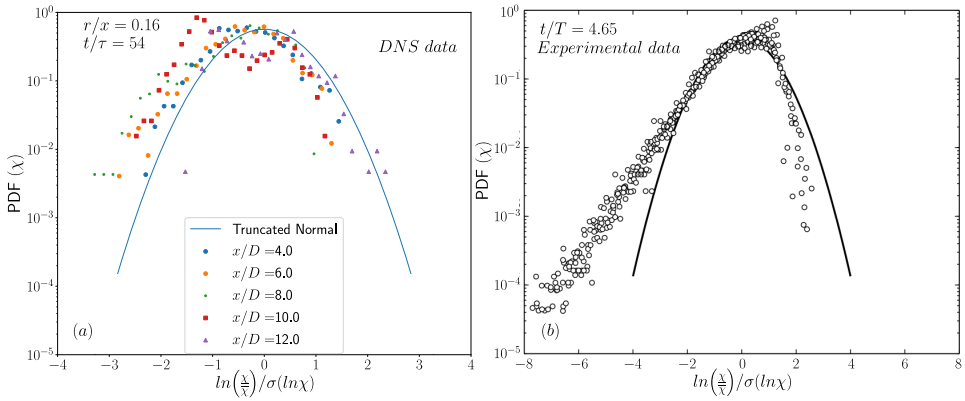

Figure 5: Probability density functions of the starting jet on the normalised logarithmic sample space of SDR at various jet locations and time instances: (a) present DNS data and (b) experimental data of Soulopoulos *et al.* (2015)

(Figure 6 *left*) and their experimental counterparts (Figure 6 *right*) show the same behaviour. However SDR values decrease faster for the experimental jet from centreline to the jet boundary.

CONCLUSIONS

Spatial characteristics of the scalar dissipation rate (SDR) are investigated using DNS of steady-state and starting turbulent round jets. The jet Reynolds number is 7 300 with an inlet Mach number of 0.304. As the scalar dissipation rate is difficult to measure experimentally, numerical simulations provide a useful tool to gain a better understanding of this essential quantity for characterising mixing between the jet and ambient fluids. For a steady-state jet, the radial profiles of the mean SDR indicate that (*i*) SDR exhibits a self-similar behaviour, and (*ii*) SDR peaks at the centreline, remains close to its maximum value up until a certain radius, then decays gradually for further radii. The profile is also consistent with previous measurements. An improved model is derived and agrees well with both the DNS data and experimental data in the self-similar region of the jet.

Radial profiles of SDR in the starting jet show increased SDR values around the leading vortices. SDR profiles then reduce in magnitude and width rapidly before recover towards the steady-state profiles as the leading vortex passes downstream.

For the steady-state jet, simple PDFs for the steady-state jet scalar dissipation show a deviation from the expected log-normal distribution, attributed to flow anisotropy. While for DNS data this is less evident, in experimental measurements the difference is significant. Despite this, PDFs at various radial and axial distances display a self-similar behaviour, with increased values scatter in the outer regions, where the jet is intermittent. The PDFs of SDR for starting jets are also found to be approximated by a log-normal distribution. Deviation from the log-normal is more visible in the case of data sampled from experimental measurements due to the wider range of sampled data.

Joint PDFs of mixture fraction and SDR display symmetry with respect to the former quantity at radial locations close to the jet centreline. At large radial distances, the symmetry is broken due to jet intermittency. This behaviour is in agreement with experimental observations. Moreover mean mixture fraction and SDR values show a decrease with increasing radii.

Understanding the mixing in non-reacting and reacting jets is dependent on an accurate description of the scalar dissipation rate. A DNS approach has been employed to characterise this important quantity, highlighting the reliability of numerical data as a complement to experimental measurements.

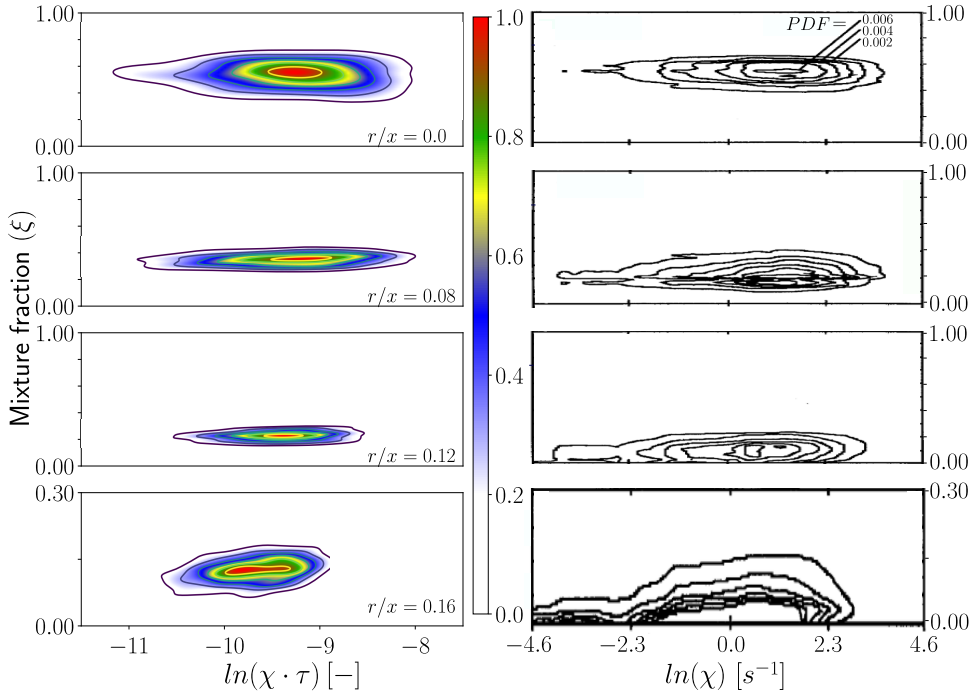

Figure 6: Joint PDF of mixture fraction (ξ) and SDR (χ) of the steady-state jet at $x/D = 14$ and different radial locations: (*left*) present DNS data and (*right*) experimental data from Feikema *et al.* (1996)

REFERENCES

Antonia, R. A., Browne, L. W. B., Chambers, A. J. & Rajagopalan, S. 1983 Budget of the temperature variance in a turbulent plane jet. *International Journal of Heat and Mass Transfer* **26** (1), 41–48.

Antonia, R. A. & Mi, J. 1993 Temperature dissipation in a turbulent round jet. *Journal of Fluid Mechanics* **250**, 531–551.

Barlow, R. S., Karpetis, A. N., Frank, J. H. & Chen, J. Y. 2001 Scalar profiles and no formation in laminar opposed-flow partially premixed methane/air flames. *Combustion and flame* **127**, 2102–2118.

Bilger, R. W. 1976 The structure of diffusion flames. *Combustion Science and Technology* **13**, 155–170.

Bremhorst, K. & Hollis, P. G. 1990 Velocity field of an axisymmetric pulsed, subsonic air jet. *AIAA journal* **28** (12), 2043–2049.

Burkardt, J. 2014 The truncated normal distribution. *Department of Scientific Computing Website, Florida State University* .

Feikema, D. A., Everest, D. & Driscoll, J. F. 1996 Images of dissipation layers to quantify mixing within a turbulent jet. *AIAA journal* **34**, 2531–2538.

Hill, W. G. & Greene, P. R. 1977 Increased turbulent jet mixing rates obtained by self-excited acoustic oscillations. *Journal of Fluids Engineering* **99** (3), 520–525.

Kaiser, S. A. & Frank, J. H. 2007 Imaging of dissipative structures in the near field of a turbulent non-premixed jet flame. *Proceedings of the Combustion Institute* **31**, 1515–1523.

Kolmogorov, A. N. 1962 A refinement of previous hypotheses concerning the local structure of turbulence in a viscous incompressible fluid at high reynolds number. *Journal of Fluid Mechanics* **13**, 82–85.

Linan, A. 1974 The asymptotic structure of counterflow diffusion flames for large activation energies. *Acta Astronautica* **1** (7-8), 1007–1039.

Mastorakos, E., B., T. A. & Poinsot, T. J. 1997 Numerical simulations of autoignition in turbulent mixing flows. *Combustion and Flame* **109**, 198–223.

Oboukhov, A. M. 1962 Some specific features of atmospheric tubulence. *Journal of Fluid Mechanics* **13**, 77–81.

Peters, N. 1984 Laminar diffusion flamelet models in non-premixed turbulent combustion. *Progress in energy and combustion science* **10**, 319–339.

Peters, N. & Williams, F. A. 1983 Liftoff characteristics of turbulent jet diffusion flames. *AIAA journal* **21**, 423–429.

Richardson, E. S., Sankaran, R., Grout, R. W. & Chen, J. H. 2010 Numerical analysis of reaction–diffusion effects on species mixing rates in turbulent premixed methane–air combustion. *Combustion and Flame* **157** (3), 506–515.

Roomina, MR & Bilger, RW 2001 Conditional moment closure (cmc) predictions of a turbulent methane-air jet flame. *Combustion and Flame* **125** (3), 1176–1195.

Sandberg, R. D. & Tester, B. J. 2016 Mach-number scaling of individual azimuthal modes of subsonic co-flowing jets. *Journal of Fluid Mechanics* **793**, 209–228.

Shin, D., Sandberg, R. D. & Richardson, E. S. 2017a Self-similarity of fluid residence time statistics in a turbulent round jet. *Journal of Fluid Mechanics* **823**, 1–25.

Soulopoulos, N., Hardalupas, Y. & Taylor, A. M. K. P. 2014 Scalar dissipation rate measurements in a starting jet. *Experiments in fluids* **55**, 1685.

Soulopoulos, N., Hardalupas, Y. & Taylor, A. M. K. P. 2015 Mixing and scalar dissipation rate statistics in a starting gas jet. *Physics of Fluids* **27** (12), 125103.

Sreenivasan, K. R., Antonia, R. A. & Danh, H. Q. 1977 Temperature dissipation fluctuations in a turbulent boundary layer. *The Physics of Fluids* **20** (8), 1238–1249.

Williams, F. A. 1975 Recent advances in theoretical descriptions of turbulent diffusion flames. In *Turbulent mixing in nonreactive and reactive flows*, pp. 189–208. Springer.